





Experimental determination of the spin Hamiltonian of the cubic chiral magnet MnSiP. Dalmas de Réotier ¹, A. Yaouanc, ¹ G. Lapertot, ¹ C. Wang ², A. Amato ², and D. Andreica ³¹*Université Grenoble Alpes, CEA, Grenoble INP, IRIG-PHELIQS, F-38000 Grenoble, France*²*Laboratory for Muon-Spin Spectroscopy, Paul Scherrer Institute, CH-5232 Villigen-PSI, Switzerland*³*Faculty of Physics, Babes-Bolyai University, 400084 Cluj-Napoca, Romania*

(Received 3 November 2023; accepted 21 December 2023; published 25 January 2024)

A thorough description of the physics of a magnetic compound requires the validation of its microscopic spin Hamiltonian. Here, from the analysis of muon-spin rotation spectra recorded in the magnetically ordered state at low temperature in zero and finite magnetic fields, we determine the minimal Hamiltonian for the chiral binary intermetallic magnet MnSi, consistent with its high-temperature nonsymmorphic cubic space group $P2_13$. The model provides constraints for the orientation of the Moriya vector characterizing the microscopic Dzyaloshinskii-Moriya interaction, with respect to the Mn nearest-neighbor bonds. Small twist and canting of the magnetic structure are revealed. Our result indicates that, within experimental uncertainties, the magnetoelastic coupling is not strong enough to lower the paramagnetic crystal symmetry in the magnetically ordered state. Additional implications from our work are discussed and complementary studies are suggested.

DOI: [10.1103/PhysRevB.109.L020408](https://doi.org/10.1103/PhysRevB.109.L020408)

Introduction. Helices appear in different systems of condensed matter and biology [1]. Sometimes rather complex patterns are formed like in the blue phases of liquid crystals [2] and the skyrmion textures in chiral magnets with B20 crystal structure [3] as first discovered for MnSi [4]. The similarity in the physics of those systems is striking [5,6].

The binary intermetallic compound MnSi is an exciting playground that is boosted by the availability of large and high purity single crystals—see, for example, Ref. [7]—and its properties can be studied in convenient temperature, magnetic field, and pressure ranges [8]. While still exotic with its lack of inversion symmetry, MnSi is a relatively simple cubic compound (nonsymmorphic space group $P2_13$) with four symmetry-equivalent manganese atoms in the unit cell. This explains the appreciable number of theoretical works published since the 1980s which have been based on a continuum description assuming a strong ferromagnetic interaction with an additional weak chiral term described by a scalar parameter [9–12]. Microscopic models have only been considered more recently [6,13–16] in a more limited number of studies.

The compound has a long experimental history beginning with the determination of its crystal structure at room temperature in 1933 [17]. Magnetic measurements indicate a magnetic phase transition at temperature $T_c \simeq 30$ K [18] with a weak first order character [19,20]. The spin structure is helicoidal according to nuclear magnetic resonance (NMR) [21].

Experimental and theoretical works [22–27] suggest MnSi to be a dual system with itinerant and localized electronic subsets. This dual picture seems to be widespread, since it applies, for example, to the ferromagnetic superconductor UGe₂ [28–30], the strange metal regime of cuprate superconductors [31], or a Ce heavy fermion system [32]. In the weak itinerant ferromagnet MnSi, the duality is thought in terms of a Hund metal, in which interorbital exchange interactions (Hund's coupling) give rise to strong ferromagnetic correlations between the electronic subsets [33,34]. This Hund metal

character could also apply to the sibling compound FeGe and explain the failure of a single subset viewpoint for this system [35].

The propagation wave vector \mathbf{k} of the magnetic structure is so small that it is most easily measured with small angle neutron scattering (SANS) [36]. This technique evidences equivalent magnetic satellites only in the vicinity of the reciprocal space origin. Hence, no conventional magnetic structure refinement can be achieved [37]. Since the original NMR and SANS measurements in 1976, the Mn magnetic moments had been assumed to draw a helix around \mathbf{k} in zero magnetic field and to form a conical phase of axis \mathbf{k} under a modest field.

This simple picture was shown in 2016 to be a first approximation to the actual structure in zero field (ZF) at low temperature [38], and later on in the conical phase near T_c [39]. This result was derived from the analysis of spectra recorded with the muon-spin-rotation (μ SR) technique, within the framework of Bertaut's representation theory for magnetic structures [40]. In particular, a ZF double-helix structure was unveiled with one of the four Mn magnetic moments of the unit cell drawing an helix along \mathbf{k} as one moves from cell to cell, while the other three moments belong to a second helix that is appreciably twisted relative to the first one.

While Bertaut's theory is nowadays a conventional tool for the determination of magnetic structures using diffraction patterns—see, for example, Refs. [41–44] for neutron data—the number of remaining free parameters after its application is still large.

Here, instead of the determination of parameters merely describing the magnetic structure, we consider a minimum nearest-neighbor spin Hamiltonian including the Heisenberg, Dzyaloshinskii-Moriya (DM), and Zeeman interactions. Assuming the possibility of small deviations from the regular helical or conical structure, a minimization of the energy is performed which imposes severe constraints on the actual

TABLE I. Coordinates of the Mn atoms in MnSi, corresponding to the equivalent sites of Wyckoff position $4a$ in space group $P2_13$. All the coordinates are expressed in unit of the lattice parameter.

γ	\mathbf{d}_γ
I	$(x_{\text{Mn}}, x_{\text{Mn}}, x_{\text{Mn}})$
II	$(\bar{x}_{\text{Mn}} + \frac{1}{2}, \bar{x}_{\text{Mn}}, x_{\text{Mn}} + \frac{1}{2})$
III	$(\bar{x}_{\text{Mn}}, x_{\text{Mn}} + \frac{1}{2}, \bar{x}_{\text{Mn}} + \frac{1}{2})$
IV	$(x_{\text{Mn}} + \frac{1}{2}, \bar{x}_{\text{Mn}} + \frac{1}{2}, \bar{x}_{\text{Mn}})$

magnetic structures. We fit the remaining free parameter to experimental μSR spectra recorded at 2 K in zero and 0.3 T fields oriented along the three principal directions of the cubic structure. This provides in turn quantitative information on the parameters entering the spin Hamiltonian, in particular, the Cartesian components of the microscopic Moriya vector.

Some basic physical properties of MnSi. The lattice parameter is $a_{\text{latt}} = 4.558 \text{ \AA}$. The Mn atoms occupy the $4a$ Wyckoff position which is entirely defined by parameter $x_{\text{Mn}} = 0.138$. As done previously [38], we shall specify the position of a unit cell by the cubic lattice vector \mathbf{i} and that of a Mn atom within a cell by \mathbf{d}_γ with $\gamma \in \{\text{I, II, III, IV}\}$. For convenience, we list the \mathbf{d}_γ coordinates in Table I.

From SANS it has been established that \mathbf{k} in ZF is collinear to one of the four threefold axes with an incommensurate modulus $k \approx 0.345 \text{ nm}^{-1}$ at low temperature [4,36,45–47]. In the conical phase, \mathbf{k} is parallel to the external magnetic field \mathbf{B}_{ext} with approximately the same modulus.

Spin Hamiltonian and its treatment. We consider classical spins \mathbf{S} interacting through the ferromagnetic Heisenberg and DM interactions. The Hamiltonian is

$$\mathcal{H} = -\frac{1}{2} \sum_{(\mathbf{i}, \mathbf{i}', \gamma, \gamma')} JS_{\mathbf{i}, \gamma} \cdot \mathbf{S}_{\mathbf{i}', \gamma'} + \frac{1}{2} \sum_{(\mathbf{i}, \mathbf{i}', \gamma, \gamma')} \mathbf{D}_{\mathbf{i}, \gamma; \mathbf{i}', \gamma'} \cdot (\mathbf{S}_{\mathbf{i}, \gamma} \times \mathbf{S}_{\mathbf{i}', \gamma'}) + \sum_{\mathbf{i}, \gamma} g\mu_B \mathbf{S}_{\mathbf{i}, \gamma} \cdot \mathbf{B}, \quad (1)$$

where the first two sums are limited to nearest neighbors (see the Supplemental Material [48]). The last quantity is the Zeeman term, in which the magnetic induction \mathbf{B} is related to \mathbf{B}_{ext} through the demagnetization field. The spectroscopic factor is set to the experimental value $g \approx 2$ [19,49]. In Eq. (1), $\mathbf{D}_{\mathbf{i}, \gamma; \mathbf{i}', \gamma'}$ represents the Moriya pseudovector (or axial vector) associated with the atomic bond between sites \mathbf{i}, γ and \mathbf{i}', γ' . It is invariant through cubic lattice translations. With four Mn spins in the unit cell and six neighbor spins for each of them, we have 24 different $\mathbf{D}_{\mathbf{i}, \gamma; \mathbf{i}', \gamma'}$ vectors. They are related to each other by the antisymmetry relation $\mathbf{D}_{\mathbf{i}, \gamma'; \mathbf{i}, \gamma} = -\mathbf{D}_{\mathbf{i}, \gamma; \mathbf{i}', \gamma'}$ and the symmetry elements of point group 23 [48]. In fact the specification of a single $\mathbf{D}_{\mathbf{i}, \gamma; \mathbf{i}', \gamma'}$ vector suffices to determine the whole set. We have chosen bond I–II as the reference bond such that $\mathbf{D}_{\mathbf{i}, \text{I}; \mathbf{i}, \text{II}} \equiv \mathbf{D} = (D^x, D^y, D^z)$ where the Cartesian components are expressed in the cubic reference frame. Note that the DM Hamiltonian can equivalently be written as the weighted sum of three antisymmetric invariants [16], the weighting factors being the \mathbf{D} components.

To lower the energy, the magnetic structure is allowed to slightly deviate from the regular helical or conical structure

through twist and canting angles. We will explicit these angles thereafter. Assuming the product ka_{latt} , the twist and canting angles, and the D^α/J ratios to be small parameters, the energy is written as an expansion up to second order in these quantities. Thanks to the incommensurate nature of the magnetic ordering, the energy minimization can be performed analytically [14,48]. It leads to

$$\frac{2}{3} \frac{-D^x + D^y - 2D^z}{J} = -ka_{\text{latt}}, \quad (2)$$

and to analytical expressions for the twist and canting angles which depend on the Mn sublattice, the orientation of \mathbf{k} and parameter

$$\frac{D^x + D^y}{J} \equiv \sigma. \quad (3)$$

The resulting magnetic structure is found consistent with the prescriptions of representation analysis, as expected. Note that Eq. (2) replaces the continuous-field model relation $k = |\mathcal{D}|/B_1$ linking k with the scalar \mathcal{D} describing the DM interaction and the exchange stiffness B_1 ; see, e.g., Ref. [9].

The polarization function. A μSR experiment gives access to a polarization function, i.e., the time evolution $P_{Z,X}(t)$ of the projection of the muon spins along the direction of the beam polarization (Z) or a direction perpendicular to \mathbf{B}_{ext} (X) [50]. As a first step towards its computation, we need an expression for Mn magnetic moment $\mathbf{m}_{\mathbf{i}, \gamma} = -g\mu_B \mathbf{S}_{\mathbf{i}, \gamma}$ at position $\mathbf{r}_{\mathbf{i}, \gamma}$. Consistently with the helical or conical magnetic structure [38,39],

$$\mathbf{m}_{\mathbf{i}, \gamma} = m_\perp [\cos(\mathbf{k}_\ell \cdot \mathbf{r}_{\mathbf{i}, \gamma}) \mathbf{a}_{\ell, \gamma} - \sin(\mathbf{k}_\ell \cdot \mathbf{r}_{\mathbf{i}, \gamma}) \mathbf{b}_{\ell, \gamma}] + \mathbf{m}_\parallel, \quad (4)$$

where \mathbf{m}_\parallel is the projection of the magnetic moment along \mathbf{B}_{ext} when a field is applied. The subscript ℓ labels one of the K-domains, and $\mathbf{a}_{\ell, \gamma}$ and $\mathbf{b}_{\ell, \gamma}$ are orthogonal unit vectors. In the regular helical and conical phases, vectors $\mathbf{a}_{\ell, \gamma}$ and $\mathbf{b}_{\ell, \gamma}$ are perpendicular to \mathbf{k}_ℓ and independent of γ . Here, we do not enforce these conditions. Instead, the minimization of the energy is obtained by allowing $\mathbf{a}_{\ell, \gamma}$ and $\mathbf{b}_{\ell, \gamma}$ to deviate from the \mathbf{a}_ℓ and \mathbf{b}_ℓ vectors of the regular structures [48], which together with \mathbf{k}_ℓ/k form a direct orthonormal basis. The vectors $\mathbf{a}_{\ell, \gamma}$ and $\mathbf{b}_{\ell, \gamma}$ are deduced from \mathbf{a}_ℓ and \mathbf{b}_ℓ after two successive rotations [14]. The first one, corresponding to a structure twist, is a rotation of angle $\omega_{\ell, \gamma}$ around \mathbf{k}_ℓ . The second one, defining the structure canting, is a rotation around an axis $\mathbf{\Gamma}_{\ell, \gamma}$ perpendicular to \mathbf{k}_ℓ .

Equipped with Eq. (4) and the prior determination of the muon crystallographic site and coupling parameter [51,52], the magnetic field vector \mathbf{B}_{loc} at the location of the probe can be derived for a given site in a given magnetic domain. Then the evolution $\mathbf{S}_\mu(t)$ of the muon spin is computed from the Larmor equation $\frac{d\mathbf{S}_\mu}{dt} = \gamma_\mu \mathbf{S}_\mu \times \mathbf{B}_{\text{loc}}$, where $\gamma_\mu = 851.6 \text{ Mrad s}^{-1} \text{ T}^{-1}$ is the muon gyromagnetic ratio. Accounting for the spin-spin and spin-lattice relaxation rates, and averaging over the crystallographically equivalent muon sites in the crystal and over the magnetic domains, the model $P_{Z,X}(t)$ functions are computed [48].

Experiments and results. The μSR experiments were carried out with single crystals grown from Czochralski pulling;

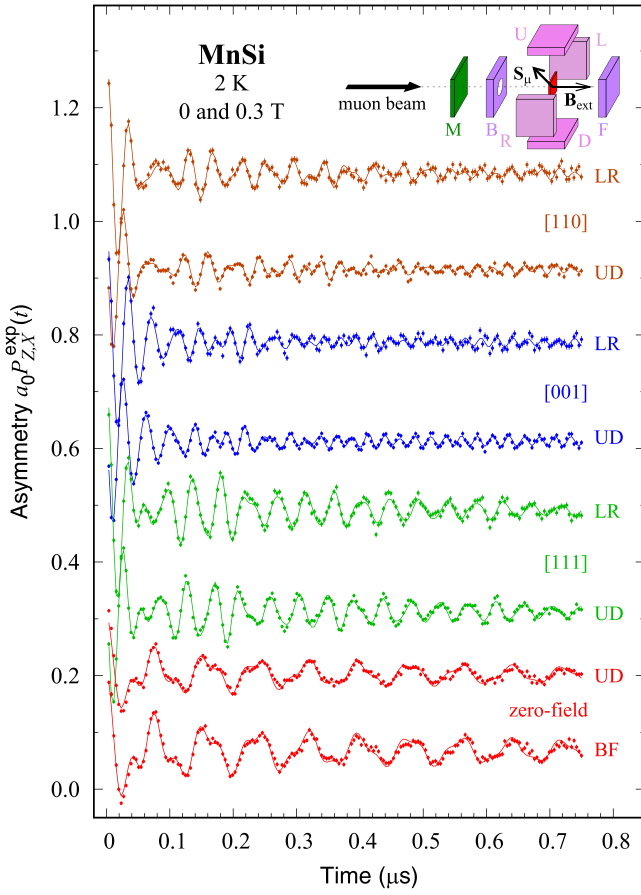


FIG. 1. μ SR spectra of a MnSi crystal at 2 K, measured either in zero field or in a 0.3 T field applied along the [111], [001], or [110] crystallographic direction as indicated in the figure. The ZF spectra obtained for the three orientations of the crystals are similar. For each measurement, the results corresponding to the relevant pair of detectors are displayed, with a vertical shift of 0.15 for better visibility. The full lines represent a combined fit to the different sets of data. The inset sketches the muon (M) and positron forward, backward, up, down, left, and right (F, B, U, D, L, R) detectors with the sample in the middle of the spectrometer. S_μ denotes the spin of the implanted muons.

see Refs. [23,52] for more details. The crystal were cut in the form of slabs oriented perpendicular to the [111], [001], or [110] cubic axes. The measurements were performed with the general purpose surface-muon (GPS) spectrometer of the Swiss muon source, Paul Scherrer Institute, Villigen, Switzerland [53]. We display in Fig. 1 the spectra recorded at 2 K in ZF and in a field of 0.3 T applied along each of the three principal directions of a cubic structure, together with the results of a fit of our model to the data. For reference, Fig. 2 presents the field distributions computed from the experimental data and fits. Overall, the description is rewarding; only near 0.2 T for the [111] direction are some details of the experimental data not captured by the model (Fig. 2).

This data analysis yields the Mn magnetic moment m and the angle of the conical structure; see Table II. As expected, the m values are reasonably independent of the field direction and intensity, and are consistent with the literature; see, e.g., Refs. [18,23,54]. The value of σ [Eq. (3)] derived from the

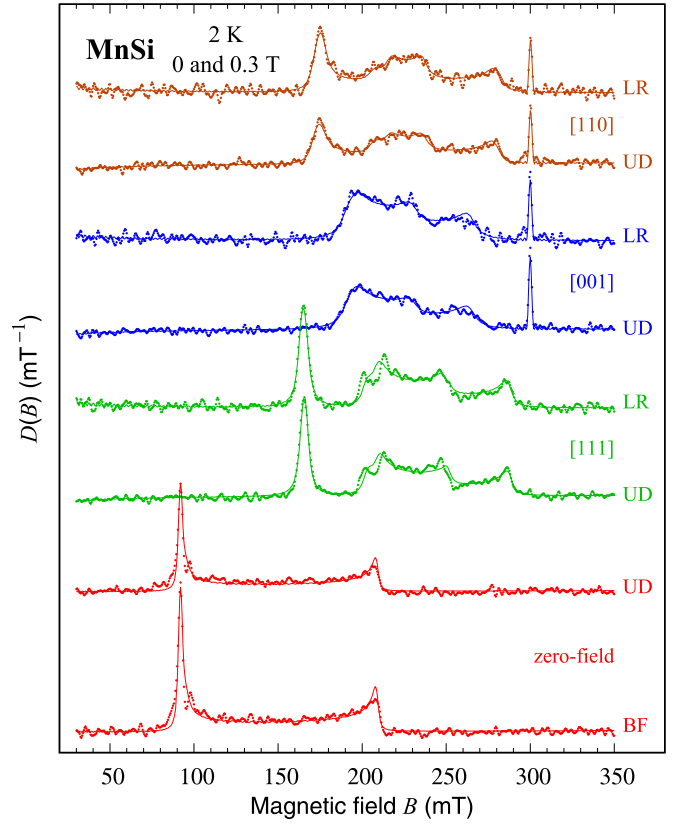


FIG. 2. Distribution of fields probed by the muons given by the Fourier transforms of the data and fits displayed in Fig. 1. The narrow peaks visible at 300 mT for the [001] and [110] spectra correspond to a background of muons stopped out of the crystal.

fit is $\sigma = 0.017(3)$. As a byproduct, we compute the twist and canting angles in ZF to be $0.83(10)$ and $0.40(7)$ degrees, respectively [48]. While a twist angle of 0.83° seems very small, it is, however, non-negligible compared to the average rotation angle 2.6° of the magnetic moments belonging to neighboring $\langle 111 \rangle$ Mn planes. The canting is approximately twice as large as found for the celebrated La_2CuO_4 case [55].

Discussion and conclusions. We first discuss the quantitative information about \mathcal{H} [Eq. (1)] derived from our analysis. As explained above, from symmetry consideration, \mathcal{H} only depends on four independent parameters: J , D^x , D^y , and D^z . A good estimate for J is provided by the analysis of the temperature dependence of m [23,26]: $J = 5.5(1)$ meV [56]. Equations (2) and (3) provide linear relations between D^x , D^y , and D^z . While a third relation linking them would be

TABLE II. Results of the combined fit to the data: Mn magnetic moment $m \approx (m_\perp^2 + m_\parallel^2)^{1/2}$ and angle $\theta = \arctan(m_\perp/m_\parallel)$ characterizing the conical structure for an applied field of 0.3 T.

Field direction	Moment m (μ_B)	Cone angle θ (deg.)
zero field	0.3881 (2)	90 (–)
[111]	0.388 (2)	66.7 (3)
[001]	0.396 (3)	63.5 (7)
[110]	0.388 (2)	66.6 (5)

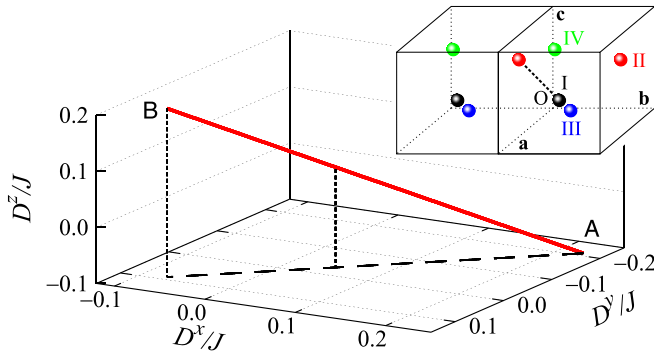


FIG. 3. Locus of the \mathbf{D} vector Cartesian coordinates resulting from the data analysis. The components are normalized to the exchange parameter J . For the sake of clarity, the projection of the line onto the $D^z/J = -0.1$ plane is shown as a dashed line. The plot is limited to $\max(|D^\alpha|/J) \lesssim 0.2$. The full line has been drawn for the nominal values of ka_{lat} and σ . Solutions in the vicinity of the line are possible according to the experimental uncertainties on each of these quantities. The vertical dotted line in the middle corresponds to the position of the minimum of D/J or of the angle between \mathbf{D} and the reference bond; see Fig. 4. The inset depicts two unit cubic cells with the four types of Mn atoms and reference bond I–II.

required for a complete determination, Fig. 3 illustrates the set of \mathbf{D} components consistent with the experimental data. The full line is obtained from the intersection of the planes defined by Eqs. (2) and (3). We note that the Moriya rules [57] provide no information on the angle between \mathbf{D} and the Mn nearest-neighbor bond, due to the absence of the requested symmetries. This is consistent with Fig. 4 for which no remarkable angle value appears. Figure 4 also displays the evolution of D/J when \mathbf{D} describes the full line of Fig. 3. Rewardingly, the condition $D/J \ll 1$ is fulfilled, which is consistent with our model.

The orientation of the Moriya vector relative to the Mn–Mn bond is closely related to the twist and canting angles. While the discussion of these angles is rare in the literature [14,16,35,58] and the present study provides an experimental

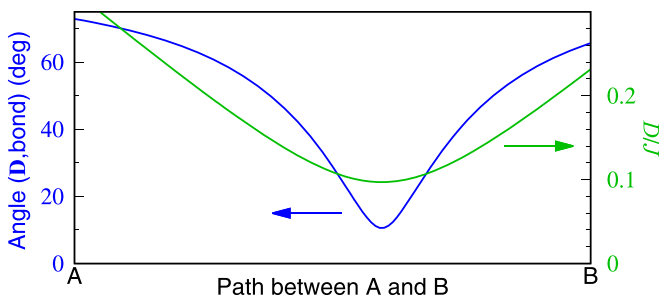


FIG. 4. Characterization of \mathbf{D} : (i) angle between the nearest-neighbor Mn atoms bond and the associated \mathbf{D} and (ii) modulus of \mathbf{D} normalized to J . Both the angle and D/J are plotted for the path between the A and B points defined in Fig. 3. As for the preceding figure, solutions in the vicinity of the two lines are possible. The minimum angle is $\simeq 10.6$ degrees.

determination of their values, the orientation of \mathbf{D} has been considered in a few theoretical works. There is no consensus.

A value $|\sigma| = 2.28$ has been estimated [59] based on a formula [60] which forces \mathbf{D} to be perpendicular to its bond, consistent with a first-principles calculation [61]. The $|\sigma|$ value is about two orders of magnitude larger than measured. A more recent *ab initio* study of MnSi has estimated the \mathbf{D} components [15]. The condition $|D^\alpha|/J \ll 1$ is satisfied, in agreement with our present results. However, with a calculated D/J ratio of approximately 1/20, \mathbf{D} is drawn roughly perpendicular to the bond. This appears inconsistent with our results, which predict the Moriya vector to be almost parallel to the bond at minimum D/J (see Fig. 4). We should also note that (i) the computed $J \approx 20$ meV value is approximately four times larger than found here [62], (ii) the Mn moment is nearly three times larger than the accepted value, and (iii) the ratio $|D^\alpha|/J$ is sizably larger for next-nearest neighbors than for nearest neighbors. In fact, MnSi is a dual system as pointed out in the introduction. Here, we describe the interactions between the Mn moment localized components. We limit ourselves to nearest-neighbor interactions, so that we work with the minimal Hamiltonian.

Remarkably, a microscopic model, but not a first-principles model, has predicted the dominant contribution to \mathbf{D} to be parallel to the corresponding bond, which is close to our experimental result when D/J is minimum [13]. Reference [6] also considers \mathbf{D} to be parallel to the bond.

The ground state energy resulting from Eq. (1) does not depend on the \mathbf{k} orientation, at least up to the second-order expansion [14,48]. While $\mathbf{k} \parallel \mathbf{B}_{\text{ext}}$ for $B_{\text{ext}} \gtrsim 0.1$ T, it is parallel to $\langle 111 \rangle$ in ZF [36]. This suggests the existence of an anisotropy term in the Hamiltonian. Two origins have been proposed: same-site energy and exchange. The former has been widely discussed [13,16,63,64]. It generates a spin gap [12]. Recalling the absence of such a gap at the sub- 10^{-7} eV level [23,26,65], the energy scale would be too small to be effective. Accounting for an exchange anisotropy would require at least one other exchange constant along with J , among a maximum of six [16]. A step forward in this direction could be a quantitative analysis of the phase diagram for which an anisotropy has been experimentally observed [66].

In conclusion, through a quantitative μSR spectra analysis, we have validated a nearest-neighbor spin Hamiltonian picture made of the sum of isotropic Heisenberg and DM terms [14,67]. Quantitative information has been derived for the Cartesian components of \mathbf{D} . An additional relation between these components is required for their full determination. Our analysis suggests the compound to be still cubic in its magnetically ordered state, in contrast to a proposal [68].

Our microscopic magnetic picture could be of interest, for example, for an insight into the partial magnetic order observed above T_c under pressure [69], or the mechanisms at play for the stabilization of the skyrmion crystal [4,68,70,71] and related topological Hall and Nernst effects [72,73]. Understanding magnetic properties in terms of the crystal structure could be crucial for magnetic engineering. The microscopic mechanism leading to $\mathbf{k} \parallel \langle 111 \rangle$ in ZF is still to be discovered. A local anisotropy can be excluded. We anticipate that the parameter σ , and therefore the ZF twist and

canting, and **D**, could be slightly different from given here when $\mathbf{k} \parallel (111)$ in ZF is explained.

Acknowledgments. We are grateful to M. Chshiev and A. Manchon for discussions about *ab initio* methods, S. Grytsiuk

for drawing our attention to Ref. [15], and A. Maisuradze for a critical reading of the manuscript. Part of this work was performed at the GPS spectrometer of the Swiss Muon Source (Paul Scherrer Institut, Villigen, Switzerland).

-
- [1] A. A. Kornyshev, D. J. Lee, S. Leikin, and A. Wynveen, Structure and interactions of biological helices, *Rev. Mod. Phys.* **79**, 943 (2007).
- [2] D. C. Wright and N. D. Mermin, Crystalline liquids: the blue phases, *Rev. Mod. Phys.* **61**, 385 (1989).
- [3] S.-W. Cheong and X. Xu, Magnetic chirality, *npj Quantum Mater.* **7**, 40 (2022).
- [4] S. Mühlbauer, B. Binz, F. Jonietz, C. Pfleiderer, A. Rosch, A. Neubauer, R. Georgii, and P. Böni, Skyrmion lattice in a chiral magnet, *Science* **323**, 915 (2009).
- [5] S. Tewari, D. Belitz, and T. R. Kirkpatrick, Blue quantum fog: Chiral condensation in quantum helimagnets, *Phys. Rev. Lett.* **96**, 047207 (2006).
- [6] A. Hamann, D. Lamago, T. Wolf, H. v. Löhneysen, and D. Reznik, Magnetic blue phase in the chiral itinerant magnet MnSi, *Phys. Rev. Lett.* **107**, 037207 (2011).
- [7] N. Doiron-Leyraud, I. R. Walker, L. Taillefer, M. J. Steiner, S. R. Julian, and G. G. Lonzarich, Fermi-liquid breakdown in the paramagnetic phase of a pure metal, *Nature (London)* **425**, 595 (2003).
- [8] D. Andreica, P. Dalmas de Réotier, A. Yaouanc, A. Amato, and G. Lapertot, Absence of magnetic phase separation in MnSi under pressure, *Phys. Rev. B* **81**, 060412(R) (2010).
- [9] P. Bak and M. H. Jensen, Theory of helical magnetic structures and phase transitions in MnSi and FeGe, *J. Phys. C* **13**, L881 (1980).
- [10] O. Nakanishi, A. Yanase, A. Hasegawa, and M. Kataoka, The origin of the helical spin density wave in MnSi, *Solid State Commun.* **35**, 995 (1980).
- [11] D. Belitz, T. R. Kirkpatrick, and A. Rosch, Theory of helimagnons in itinerant quantum systems, *Phys. Rev. B* **73**, 054431 (2006).
- [12] S. V. Maleyev, Cubic magnets with Dzyaloshinskii-Moriya interaction at low temperature, *Phys. Rev. B* **73**, 174402 (2006).
- [13] J. M. Hopkinson and H.-Y. Kee, Origin and consequences of unpinned helical order: Application to MnSi under pressure, *Phys. Rev. B* **79**, 014421 (2009).
- [14] V. A. Chizhikov and V. E. Dmitrienko, Frustrated magnetic helices in MnSi-type crystals, *Phys. Rev. B* **85**, 014421 (2012).
- [15] V. Borisov, Y. O. Kvasninin, N. Ntallis, D. Thonig, P. Thunström, M. Pereiro, A. Bergman, E. Sjöqvist, A. Delin, L. Nordström, and O. Eriksson, Heisenberg and anisotropic exchange interactions in magnetic materials with correlated electronic structure and significant spin-orbit coupling, *Phys. Rev. B* **103**, 174422 (2021).
- [16] K. P. W. Hall and S. H. Curnoe, Generalized model of MnSi-like spiral magnets, *Phys. Rev. B* **104**, 094408 (2021).
- [17] B. Borén, Roentgenuntersuchung der legierungen von silicium mit chrom, mangan, kobalt und nickel, *Ark. Kemi Mineral. Geol.* **11A**, 1 (1933).
- [18] H. J. Williams, J. H. Wernick, R. C. Sherwood, and G. K. Wertheim, Magnetic properties of the monosilicides of some 3d transition elements, *J. Appl. Phys.* **37**, 1256 (1966).
- [19] M. Date, K. Okuda, and K. Kadowaki, Electron spin resonance in the itinerant-electron helical magnet MnSi, *J. Phys. Soc. Jpn.* **42**, 1555 (1977).
- [20] S. M. Stishov, A. E. Petrova, S. Khasanov, G. K. Panova, A. A. Shikov, J. C. Lashley, D. Wu, and T. A. Lograsso, Magnetic phase transition in the itinerant helimagnet MnSi: Thermodynamic and transport properties, *Phys. Rev. B* **76**, 052405 (2007).
- [21] K. Motoya, H. Yasuoka, Y. Nakamura, and J. H. Wernick, Helical spin structure in MnSi-NMR studies, *Solid State Commun.* **19**, 529 (1976).
- [22] K. R. A. Ziebeck, H. Capellmann, P. J. Brown, and J. G. Booth, Spin fluctuations in both the ordered and paramagnetic phases of MnSi! MnSi a heavy Fermi liquid? *Z. Phys. B* **48**, 241 (1982).
- [23] A. Yaouanc, P. Dalmas de Réotier, B. Roessli, A. Maisuradze, A. Amato, D. Andreica, and G. Lapertot, Dual nature of magnetism in MnSi, *Phys. Rev. Res.* **2**, 013029 (2020).
- [24] X. Chen, I. Krivenko, M. B. Stone, A. I. Kolesnikov, T. Wolf, D. Reznik, K. S. Bedell, F. Lechermann, and S. D. Wilson, Unconventional Hund metal in a weak itinerant ferromagnet, *Nat. Commun.* **11**, 3076 (2020).
- [25] H. Choi, Y.-Y. Tai, and J.-X. Zhu, Spin-fermion model for skyrmions in MnGe derived from strong correlations, *Phys. Rev. B* **99**, 134437 (2019).
- [26] P. Dalmas de Réotier and A. Yaouanc, Zero-field ^{29}Si nuclear magnetic resonance signature of helimagnons in MnSi, *J. Magn. Mater.* **537**, 168086 (2021).
- [27] Y. Fang, H. Zhang, D. Wang, G. Yang, Y. Wu, P. Li, Z. Xiao, T. Lin, H. Zheng, X.-L. Li, H.-H. Wang, F. Rodolakis, Y. Song, Y. Wang, C. Cao, and Y. Liu, Quasiparticle characteristics of the weakly ferromagnetic Hund metal MnSi, *Phys. Rev. B* **106**, L161112 (2022).
- [28] A. Yaouanc, P. Dalmas de Réotier, P. C. M. Gubbens, C. T. Kaiser, A. A. Menovsky, M. Mihalik, and S. P. Cottrell, Evidence for weak itinerant long-range magnetic correlations in UGe_2 , *Phys. Rev. Lett.* **89**, 147001 (2002).
- [29] S. Sakarya, P. C. M. Gubbens, A. Yaouanc, P. Dalmas de Réotier, D. Andreica, A. Amato, U. Zimmermann, N. H. van Dijk, E. Brück, Y. Huang, and T. Gortenmulder, Positive muon spin rotation and relaxation measurements on the ferromagnetic superconductor UGe_2 at ambient and high pressure, *Phys. Rev. B* **81**, 024429 (2010).
- [30] F. Haslbeck, S. Säubert, M. Seifert, C. Franz, M. Schulz, A. Heinemann, T. Keller, P. Das, J. D. Thompson, E. D. Bauer, C. Pfleiderer, and M. Janoschek, Ultrahigh-resolution neutron spectroscopy of low-energy spin dynamics in UGe_2 , *Phys. Rev. B* **99**, 014429 (2019).
- [31] J. Ayres, M. Berben, M. Čulo, Y.-T. Hsu, E. van Heumen, Y. Huang, J. Zaanen, T. Kondo, T. Takeuchi, J. R. Cooper, C.

- Putzke, S. Friedemann, A. Carrington, and N. E. Hussey, Incoherent transport across the strange-metal regime of overdoped cuprates, *Nature (London)* **595**, 661 (2021).
- [32] K. Machida, Violation of the Pauli-Clogston limit in the heavy fermion superconductor CeRh₂As₂: Duality of itinerant and localized $4f$ electrons, *Phys. Rev. B* **106**, 184509 (2022).
- [33] A. Georges, L. de' Medici, and J. Mravlje, Strong correlations from Hund's coupling, *Annu. Rev. Condens. Matter Phys.* **4**, 137 (2013).
- [34] Y. Nomura, S. Sakai, and R. Arita, Fermi surface expansion above critical temperature in a Hund ferromagnet, *Phys. Rev. Lett.* **128**, 206401 (2022).
- [35] S. Grytsiuk, M. Hoffmann, J.-P. Hanke, P. Mavropoulos, Y. Mokrousov, G. Bihlmayer, and S. Blügel, *Ab initio* analysis of magnetic properties of the prototype B20 chiral magnet FeGe, *Phys. Rev. B* **100**, 214406 (2019).
- [36] Y. Ishikawa, K. Tajima, D. Bloch, and M. Roth, Helical spin structure in manganese silicide MnSi, *Solid State Commun.* **19**, 525 (1976).
- [37] J. Rossat-Mignod, in *Neutron Scattering*, Methods of Experimental Physics Vol. 23, Part C, edited by K. Sköld and D. L. Price (Academic, New York, 1987).
- [38] P. Dalmas de Réotier, A. Maisuradze, A. Yaouanc, B. Roessli, A. Amato, D. Andreica, and G. Lapertot, Determination of the zero-field magnetic structure of the helimagnet MnSi at low temperature, *Phys. Rev. B* **93**, 144419 (2016).
- [39] P. Dalmas de Réotier, A. Maisuradze, A. Yaouanc, B. Roessli, A. Amato, D. Andreica, and G. Lapertot, Unconventional magnetic order in the conical state of MnSi, *Phys. Rev. B* **95**, 180403(R) (2017).
- [40] E. F. Bertaut, in *Treatise on Magnetism*, edited by H. Suhl and G. T. Rado (Academic, New York, 1963), Vol. III, Chap. 4; Representation analysis of magnetic structures, *Acta Crystallogr. A* **24**, 217 (1968); Magnetic structure analysis and group theory, *J. Phys. Colloques* **32**, C1-462 (1971); On group theoretical techniques in magnetic structure analysis, *J. Magn. Magn. Mater.* **24**, 267 (1981).
- [41] A. S. Wills, Magnetic structures and their determination using group theory, *J. Phys. IV France* **11**, Pr9-133 (2001).
- [42] M. Kenzelmann, A. B. Harris, A. Aharony, O. Entin-Wohlman, T. Yildirim, Q. Huang, S. Park, G. Lawes, C. Broholm, N. Rogado, R. J. Cava, K. H. Kim, G. Jorge, and A. P. Ramirez, Field dependence of magnetic ordering in kagomé-staircase compound Ni₃V₂O₈, *Phys. Rev. B* **74**, 014429 (2006).
- [43] M. Kenzelmann, T. Strässle, C. Niedermayer, M. Sigrist, B. Padmanabhan, M. Zolliker, A. D. Bianchi, R. Movshovich, E. D. Bauer, J. L. Sarrao, and J. D. Thompson, Coupled superconducting and magnetic order in CeCoIn₅, *Science* **321**, 1652 (2008).
- [44] J. Rodríguez-Carvajal and J. Villain, Magnetic structures, *C. R. Phys.* **20**, 770 (2019).
- [45] M. Ishida, Y. Endoh, S. Mitsuda, Y. Ishikawa, and M. Tanaka, Crystal chirality and helicity of the helical spin density wave in MnSi. II. Polarized neutron diffraction, *J. Phys. Soc. Jpn.* **54**, 2975 (1985).
- [46] B. Fåk, R. A. Sadykov, J. Flouquet, and G. Lapertot, Pressure dependence of the magnetic structure of the itinerant electron magnet MnSi, *J. Phys.: Condens. Matter* **17**, 1635 (2005).
- [47] S. V. Grigoriev, S. V. Maleyev, A. I. Okorokov, Y. O. Chetverikov, P. Böni, R. Georgii, D. Lamago, H. Eckerlebe, and K. Pranzas, Magnetic structure of MnSi under an applied field probed by polarized small-angle neutron scattering, *Phys. Rev. B* **74**, 214414 (2006).
- [48] See Supplemental Material at <http://link.aps.org/supplemental/10.1103/PhysRevB.109.L020408> for details on the derivation of the magnetic structure from the minimization of the energy, the computation of the polarization functions, and a comparison with a former model; see also Refs. [74–77] cited therein.
- [49] S. V. Demishev, A. V. Semeno, A. V. Bogach, V. V. Glushkov, N. E. Sluchanko, N. A. Samarin, and A. L. Chernobrovkin, Is MnSi an itinerant electron magnet? Results of ESR experiments, *JETP Lett.* **93**, 213 (2011).
- [50] A. Yaouanc and P. Dalmas de Réotier, *Muon Spin Rotation, Relaxation, and Resonance: Applications to Condensed Matter* (Oxford University Press, Oxford, 2011).
- [51] A. Amato, P. Dalmas de Réotier, D. Andreica, A. Yaouanc, A. Suter, G. Lapertot, I. M. Pop, E. Morenzoni, P. Bonfà, F. Bernardini, and R. De Renzi, Understanding the μ SR spectra of MnSi without magnetic polarons, *Phys. Rev. B* **89**, 184425 (2014).
- [52] P. Dalmas de Réotier, A. Yaouanc, A. Amato, A. Maisuradze, D. Andreica, B. Roessli, T. Goko, R. Scheuermann, and G. Lapertot, On the robustness of the MnSi magnetic structure determined by muon spin rotation, *Quantum Beam Sci.* **2**, 19 (2018).
- [53] A. Amato, H. Luetkens, K. Sedlak, A. Stoykov, R. Scheuermann, M. Elender, A. Raselli, and D. Graf, The new versatile general purpose surface-muon instrument (GPS) based on silicon photomultipliers for μ SR measurements on a continuous-wave beam, *Rev. Sci. Instrum.* **88**, 093301 (2017).
- [54] J. H. Wernick, G. K. Wertheim, and R. C. Sherwood, Magnetic behavior of the monosilicides of the 3d-transition elements, *Mater. Res. Bull.* **7**, 1431 (1972).
- [55] T. Thio, T. R. Thurston, N. W. Preyer, P. J. Picone, M. A. Kastner, H. P. Jenssen, D. R. Gabbe, C. Y. Chen, R. J. Birgeneau, and A. Aharony, Antisymmetric exchange and its influence on the magnetic structure and conductivity of La₂CuO₄, *Phys. Rev. B* **38**, 905 (1988).
- [56] In Ref. [23] a continuous field model is used with a stiffness denoted as B_1 . It is related to J through $J = 4\mathcal{J}/3a_{\text{fitt}}^2$ [14] with $\mathcal{J} \equiv B_1/2$. Numerically, from $B_1 = 2.73(4) \times 10^{-40} \text{ J m}^2$, $J = 8.8(1) \times 10^{-22} \text{ J}$.
- [57] T. Moriya, Anisotropic superexchange interaction and weak ferromagnetism, *Phys. Rev.* **120**, 91 (1960).
- [58] S. Grytsiuk and S. Blügel, Micromagnetic description of twisted spin spirals in the B20 chiral magnet FeGe from first principles, *Phys. Rev. B* **104**, 064420 (2021).
- [59] V. E. Dmitrienko and V. A. Chizhikov, Weak antiferromagnetic ordering induced by Dzyaloshinskii-Moriya interaction and pure magnetic reflections in MnSi-type crystals, *Phys. Rev. Lett.* **108**, 187203 (2012).
- [60] F. Keffer, Moriya interaction and the problem of the spin arrangements in β MnS, *Phys. Rev.* **126**, 896 (1962).
- [61] M. I. Katsnelson, Y. O. Kvashnin, V. V. Mazurenko, and A. I. Lichtenstein, Correlated band theory of spin and orbital contributions to Dzyaloshinskii-Moriya interactions, *Phys. Rev. B* **82**, 100403(R) (2010).
- [62] Note the difference between the convention of Ref. [15] and ours: the factors 1/2 of Eq. (1) are absent in the quoted reference.

- [63] S. V. Grigoriev, A. S. Sukhanov, and S. V. Maleyev, From spiral to ferromagnetic structure in B20 compounds: Role of cubic anisotropy, *Phys. Rev. B* **91**, 224429 (2015).
- [64] V. A. Chizhikov, Anisotropy of the magnetic phases in cubic helimagnets, *J. Exp. Theor. Phys.* **132**, 559 (2021).
- [65] A. Yaouanc, P. Dalmas de Réotier, P. C. M. Gubbens, S. Sakarya, G. Lapertot, A. D. Hillier, and P. J. C. King, Testing the self-consistent renormalization theory for the description of the spin-fluctuation modes of MnSi at ambient pressure, *J. Phys.: Condens. Matter* **17**, L129 (2005).
- [66] M. Ohkuma, M. Mito, M. Pardo, Y. Kousaka, S. Iwasaki, K. Ohishi, J. Akimitsu, K. Inoue, V. Laliena, and J. Campo, New magnetic intermediate state, “B-phase,” in the cubic chiral magnet MnSi, *APL Mater.* **10**, 041104 (2022).
- [67] A first approach to the determination of a spin Hamiltonian using μ SR data has been presented in H. Maeter, H. Luetkens, Y. G. Pashkevich, A. Kwadrin, R. Khasanov, A. Amato, A. A. Gusev, K. V. Lamonova, D. A. Chervinskii, R. Klingeler, C. Hess, G. Behr, B. Büchner, and H.-H. Klauss, Interplay of rare earth and iron magnetism in RFeAsO ($R = \text{La, Ce, Pr, and Sm}$): Muon-spin relaxation study and symmetry analysis, *Phys. Rev. B* **80**, 094524 (2009).
- [68] A. B. Butenko, A. A. Leonov, U. K. Rößler, and A. N. Bogdanov, Stabilization of skyrmion textures by uniaxial distortions in noncentrosymmetric cubic helimagnets, *Phys. Rev. B* **82**, 052403 (2010).
- [69] C. Pfleiderer, D. Reznik, L. Pintschovius, H. v. Löhneysen, M. Garst, and A. Rosch, Partial order in the non-Fermi-liquid phase of MnSi, *Nature (London)* **427**, 227 (2004).
- [70] A. N. Bogdanov and D. A. Yablonskii, Thermodynamically stable “vortices” in magnetically ordered crystals. The mixed state of magnets, *Sov. Phys. JETP* **68**, 101 (1989).
- [71] A. Bogdanov and A. Hubert, Thermodynamically stable magnetic vortex states in magnetic crystals, *J. Magn. Magn. Mater.* **138**, 255 (1994).
- [72] A. Neubauer, C. Pfleiderer, B. Binz, A. Rosch, R. Ritz, P. G. Niklowitz, and P. Böni, Topological Hall effect in the A phase of MnSi, *Phys. Rev. Lett.* **102**, 186602 (2009).
- [73] H. Oike, T. Ebino, T. Koretsune, A. Kikkawa, M. Hirschberger, Y. Taguchi, Y. Tokura, and F. Kagawa, Topological Nernst effect emerging from real-space gauge field and thermal fluctuations in a magnetic skyrmion lattice, *Phys. Rev. B* **106**, 214425 (2022).
- [74] P. Dalmas de Réotier and A. Yaouanc, Muon spin rotation and relaxation in magnetic materials, *J. Phys.: Condens. Matter* **9**, 9113 (1997).
- [75] P. P. Ewald, Die Berechnung optischer und elektrostatischer Gitterpotentiale, *Ann. Phys. (Leipzig)* **369**, 253 (1921).
- [76] M. Born and K. Huang, *Dynamical Theory of Crystal Lattices* (Clarendon, Oxford, 1954).
- [77] A. Yaouanc, P. Dalmas de Réotier, and E. Frey, Zero-field muon-spin-relaxation depolarization rate of paramagnets near the Curie temperature, *Phys. Rev. B* **47**, 796 (1993).